THE JET/CGC CORRESPONDENCE: A CONFORMAL PERSPECTIVE*

J.A. Bohra, Heribert Weigert

University of Cape Town, Rondebosch, 7700, Cape Town, South Africa

Received 14 February 2023, accepted 24 August 2023, published online 27 October 2023

In recent years, there has been a concerted effort to formalize the many similarities between jet evolution, which models high-energy particle production experiments, and CGC evolution, which models high-energy scattering experiments. In this paper, the spatial correspondence of kernels and measures in both evolution equations and the spacetime correspondence of Wilson line geometries have been discussed in terms of conformal transformations.

DOI:10.5506/APhysPolBSupp.16.8-A16

1. Introduction

The theoretical correspondence of the BK [1] and BMS [2] equations is not entirely surprising; their respective derivations share technical similarities: both are derived in the 't Hooft large-N_c limit of the Yang–Mills theory, both employ eikonalized soft emission techniques in a strongly ordered setting [3], and both track 1-loop contributions to the inclusive Deep Inelastic Scattering and semi-inclusive e^+e^- annihilation cross sections, respectively, through the *hardest* soft gluon — albeit in deeply spacelike and deeply timelike kinematics, respectively.

Phenomenologically, where the BK equation characterizes evolution of the Colour Glass Condensate, the BMS equation characterizes evolution of jets. Their phenomenological correspondence shall be studied through a stereographic projection by Hatta [4] and conformal spacetime map presented by Hofman and Maldacena [5].

2. The Colour Glass Condensate

Kinematics of Deep Inelastic Scattering (DIS) events may be characterized by the t-channel interaction of spacelike photon γ_* (with momentum q^μ)

* Presented at *Excited QCD 2022*, Sicily, Italy, 23–29 October, 2022.

and a hadron (with momentum P^μ). Momentum transfer between photon and hadron is quantified by a scaleless momentum fraction $x_{\rm Bj}$. Spatial resolution of hadronic constituents (collectively called partons) probed is quantified by Q^2 — which is inversely proportional to the transverse area of partons $Q^2 \sim 1/A_\perp$. The kinematics of DIS events are characterized by

$$Q^2 := -q^\mu q_\mu \,, \qquad x_{\rm Bj} := \frac{-q^2}{2P\cdot q} \in [0,1)\,. \tag{1}$$

At fixed $x_{\rm Bj}$, probing the hadron at higher Q^2 increases hadronic occupation at finer resolutions [6] so that the hadron is viewed as a dilute collection of partons, as shown in figure 1 (a) moving rightward. Analogously, at fixed Q^2, probing the hadron at lower $x_{\rm Bj}$ increases hadronic occupation at fixed resolution — known as the Regge–Gribov limit as shown in figure 1 (a) moving upward. Beyond the saturation scale $\ln 1/x_{\rm Bj} = \ln Q_s^2$, the hadron becomes saturated with partons (mainly gluons as evidenced by HERA data [7]). Individual gluons cannot be resolved in the saturation regime. What arises is a universal state of matter that describes the high gluon density part of the hadronic wavefunction at small $x_{\rm Bj}$ — namely, the Color Glass Condensate (CGC) [8].

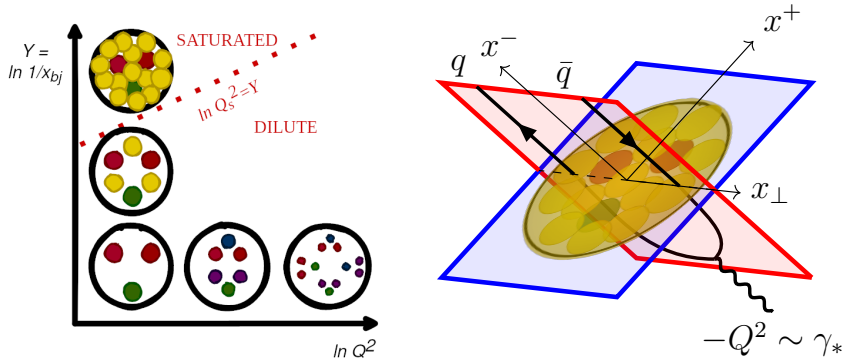

(a) QCD phase space (b) Spacetime diagram

Fig. 1. (Colour on-line) Partonic behaviour of the hadron characterized in terms of $x_{\rm Bj}$ and Q^2 in (a). Kinematics hadron and virtual photon interaction of DIS amplitude in the Regge–Gribov limit depicted in (b); Photon splits into hard quark–antiquark pair $\gamma_* \to q\bar{q}$ and lightcone coordinate axes depicted.

At small $x_{\rm Bj}$, $Y \simeq \ln 1/x_{\rm Bj}$, where Y is the rapidity of interaction [1]. The kinematics of DIS in the Regge–Gribov limit must be reflected in the gluonic dynamics of the CGC which are governed by the non-Abelian gauge field $b^{\mu a}(x) = \bar{n}^\mu \delta(x^-)\beta^a(\boldsymbol{x}_\perp)$ [8] expressed in lightcone coordinates of the

Kogut–Soper convention [9], $x^\mu = x^+\bar{n}^\mu + x_\perp^\mu + x^- n^\mu$ such that $n \cdot \bar{n} = 1$. The simplest QCD interaction between photon and hadron involves the amplitude $\gamma_* \to q\bar{q}$, see figure 1 (b). In figure 1 (b), the $\gamma_* \to q\bar{q}$ (traversing the x^- coordinate) and the hadronic target (traversing the x^+ coordinate) are depicted on the red/light gray and blue/gray lightsheets respectively. Formally, the colour rotation of the colour part of the partonic wavefunctions is enacted through the Wilson lines along a straight path

$$U_{x;f,i} := P \exp\left[(-ig)\int_i^f \mathrm{d}x^- n_\mu b^{\mu a}(x) t^a_{(\mathrm{rep})}\right] . \tag{2}$$

3. Theoretical correspondence of jet/CGC evolution

The cross section of the $\gamma_* \to q\bar{q}$ amplitude depicted in figure 1 (b) has been computed in the literature [1]. All x_{Bj} dependence of the cross section is carried by the Wilson line correlator

$$S_{xy}(x_{\mathrm{Bj}}) := \frac{\left\langle \mathrm{tr}\left(U_x U_y^\dagger\right)\right\rangle (x_{\mathrm{Bj}})}{N_{\mathrm{c}}} . \tag{3}$$

Explicitly x_{Bj} dependence is deduced through the BK equation showcased in Eq. (4a). Note that x, y, and z denote coordinates of the quark, antiquark, and emitted soft gluon used to track the 1-loop correction to S_{xy}, in Eq. (3), respectively. The kernel K_{xzy} is a transverse spatial coordinate-dependent rational function. The transverse coordinate of the emitted soft gluon is integrated over $\int \mathrm{d}^2\boldsymbol{z}_\perp$

$$\frac{\mathrm{d}}{\mathrm{d}\ln(1/x_{\mathrm{Bj}})} S_{xy}(x_{\mathrm{Bj}}) = \frac{\alpha_{\mathrm{s}} N_{\mathrm{c}}}{\pi}\int \frac{\mathrm{d}^2\boldsymbol{z}_\perp}{2\pi} K_{xzy}\left\{S_{xz}(x_{\mathrm{Bj}}) S_{zy}(x_{\mathrm{Bj}}) - S_{xy}(x_{\mathrm{Bj}})\right\} , \tag{4a}$$

$$\begin{aligned}\frac{\mathrm{d}}{\mathrm{d}\ln(E/E_{\mathrm{out}})} G_{pq}(E) = {} & \frac{\alpha_{\mathrm{s}} N_{\mathrm{c}}}{\pi}\int \frac{\mathrm{d}^2\hat{\boldsymbol{k}}}{4\pi} W_{pkq}[u(k)]\left\{G_{pk}(E) G_{kq}(E) - G_{pq}(E)\right\} \\ & - \frac{\alpha_{\mathrm{s}} N_{\mathrm{c}}}{\pi}\int \frac{\mathrm{d}^2\hat{\boldsymbol{k}}}{4\pi} W_{pkq}[1-u(k)] G_{pq}(E) .\end{aligned} \tag{4b}$$

The BK equation demonstrates remarkable similarity with the BMS equation (showcased in Eq. (4b)) [2]. The BMS equation tracks the energy dependence E of a semi-inclusive jet measurement. Note that $\gamma^* \to q\bar{q}$, where γ^* is a deeply timelike virtual photon. The energy E is treated as a variable and approximates the hard scale $E \sim Q$. Note that p, q, and k

denote momenta of the quark, antiquark, and emitted soft gluon used to track the 1-loop correction to the $G_{pq}(E)$ respectively. The kernel W_{pkq} is a scaleless momentum-direction-dependent rational function. The direction of the emitted soft gluon is integrated over with the surface integral $\int \mathrm{d}^2\hat{\boldsymbol{k}}$.

Structural similarities between the BK and BMS equations are showcased in Eq. (4b), the interpretation of the distribution $G_{pq}(E)$ as a Wilson line correlator [10] is like in Eq. (3),

$$G_{pq}(E) \overset{!}{:=} \frac{\langle \mathrm{tr}(\mathcal{V}_p \mathcal{V}_q)\rangle(E)}{N_\mathrm{c}} \,. \tag{5}$$

The Wilson lines in the N_c jet evolution equation manifest as

$$\mathcal{V}_p := V_p V_p' \,, \tag{6}$$

where V_p and V_p' are half-infinite Wilson lines, arising respectively from the amplitude $\gamma^* \to q\bar{q}$ and complex conjugate thereof. The Wilson lines traverse lightlike trajectories $p^\mu = \omega_p \hat{p}^\mu$ on the green/light gray forward lightcone, see figure 2.

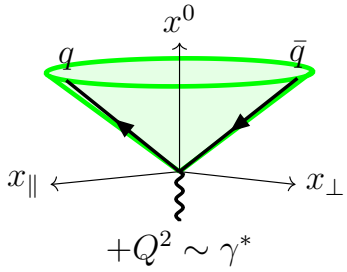

Fig. 2. (Colour on-line) Spacetime diagram demonstrating timelike photon splitting into a hard quark–antiquark pair; lightcone trajectories depicted.

4. Interjet energy observable

Phenomenologically, the study of interjet hadronic emission, which originates from the colour flow between jets, is important for understanding mechanisms of colour neutralization [2]. The interjet energy observable

$$E_\mathrm{out} = \sum_{h \in \mathcal{C}_\mathrm{out}} \omega_h \,, \tag{7}$$

where is ω_h is the energy of a single hadron in the final state. The jet region $\mathcal{C}_\mathrm{in}$ where all hard jets are focussed and, the associated complement, the interjet region $\mathcal{C}_\mathrm{out}$ help enact a semi-inclusive measurement of the final-state particles. For a given interjet region $\mathcal{C}_\mathrm{out}$ and a veto energy E_veto, all

events, where $E_{\text{out}} > E_{\text{veto}}$ are discarded, see figure 3 (a). In Eq. (4b), the effect of the veto is enacted through $u(k) := \Theta_{\text{in}}(k) + \mathrm{e}^{-\omega/E_{\text{out}}}\Theta_{\text{out}}(k)$, where the Heavisides are defined such that their supports correspond to $\mathcal{C}_{\text{in}}$ and $\mathcal{C}_{\text{out}}$ respectively. The interjet energy veto introduces a bias toward high thrust events as showcased in figures 3 (b) and 3 (c).

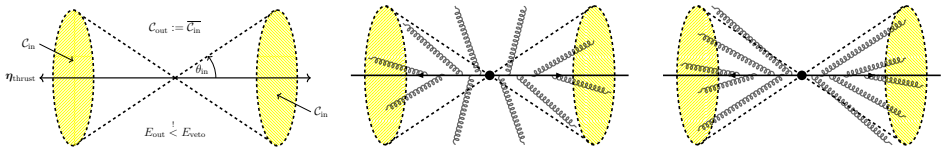

(a) Schematic of E_{out} (b) Low thrust (c) High thrust

Fig. 3. Interjet energy observable detailed in (a). Low thrust events admit more final-state particles to interjet region in (b) and *vice versa* in (c).

5. Relating kernels and measures

Weigert [10] suggested geometric identification prescription in relating the transverse plane with the sphere of directions, $\mathrm{d}^2\hat{\boldsymbol{k}} W_{pkq} \overset{?}{\leftrightarrow} \mathrm{d}^2\boldsymbol{z}_\perp K_{xzy}$, which was concretized via a stereographic projection by Hatta [4]

$$\boldsymbol{\sigma} : \boldsymbol{z}_\perp \mapsto \frac{2z^1}{1+\boldsymbol{z}_\perp^2}\boldsymbol{e}_1 - \frac{2z^2}{1+\boldsymbol{z}_\perp^2}\boldsymbol{e}_2 - \frac{1-\boldsymbol{z}_\perp^2}{1+\boldsymbol{z}_\perp^2}\boldsymbol{e}_3 \overset{!}{=} \hat{k}^1\boldsymbol{e}_1 + \hat{k}^2\boldsymbol{e}_2 + \hat{k}^3\boldsymbol{e}_3\,. \quad (8)$$

As a locally bijective map,

$$\boldsymbol{\sigma} : \{\boldsymbol{x}_\perp, \boldsymbol{y}_\perp, \boldsymbol{z}_\perp\} \to \left\{\hat{\boldsymbol{p}}, \hat{\boldsymbol{q}}, \hat{\boldsymbol{k}}\right\}, \quad (9)$$

the stereographic projection maps transverse coordinates to angular directions uniquely, see figure 4.

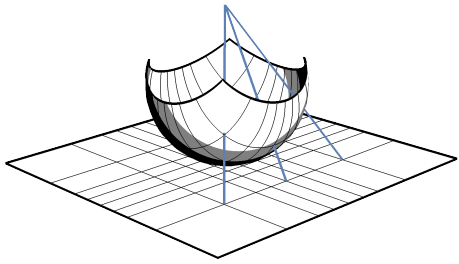

Fig. 4. Parametric mesh plot showing $\boldsymbol{\rho}_\perp \mapsto \boldsymbol{\sigma}(\boldsymbol{\rho}_\perp)$ for $\boldsymbol{\rho}_\perp \in [-2,+2]^2$.

Through $\boldsymbol{\sigma}$, it is established

$$\mathrm{d}^2\hat{\boldsymbol{k}} = \left(\frac{2}{1+\boldsymbol{z}_\perp^2}\right)^2 \mathrm{d}^2\boldsymbol{z}_\perp\,, \quad \text{and} \quad 1-\hat{\boldsymbol{p}}\cdot\hat{\boldsymbol{q}} = \frac{2\,(\boldsymbol{x}_\perp-\boldsymbol{y}_\perp)^2}{\left(1+\boldsymbol{x}_\perp^2\right)\left(1+\boldsymbol{y}_\perp^2\right)}\,. \tag{10}$$

The measures and kernels of Eq. (4b) are related $\frac{\mathrm{d}^2\hat{\boldsymbol{k}}}{4\pi}W_{pkq} = \frac{\mathrm{d}^2\boldsymbol{z}_\perp}{2\pi}K_{xzy}$,

$$\frac{\mathrm{d}^2\hat{\boldsymbol{k}}}{4\pi}\frac{(1-\hat{\boldsymbol{p}}\cdot\hat{\boldsymbol{q}})}{\left(1-\hat{\boldsymbol{p}}\cdot\hat{\boldsymbol{k}}\right)\left(1-\hat{\boldsymbol{k}}\cdot\hat{\boldsymbol{q}}\right)} = \frac{\mathrm{d}^2\boldsymbol{z}_\perp}{2\pi}\frac{(\boldsymbol{x}_\perp-\boldsymbol{y}_\perp)^2}{(\boldsymbol{x}_\perp-\boldsymbol{z}_\perp)^2(\boldsymbol{z}_\perp-\boldsymbol{y}_\perp)^2}\,. \tag{11}$$

6. Relating Wilson line trajectories

Using developments from [5, 11], a conformal map shall be used to relate the red/light gray lightsheet in figure 1 (b) to the green/light gray lightcone in figure 2. Using translations and special conformal transformations, one defines $\mathrm{c} : T_{[+n/\sqrt{2}]} \circ \Sigma_{[-\bar{n}\sqrt{2}]} \circ T_{[+n(1/\sqrt{2}-\lambda)]}$, where λ observes the function of regulator

$$\mathrm{c}^\mu(x) = \Omega_\mathrm{c} n_\mathrm{c}^\mu + x^+\bar{n}_\mathrm{c}^\mu := \left(\frac{1}{2(\lambda-x^-)}\right)\left(-x_\perp^2\bar{n}^\mu + \sqrt{2}x_\perp^\mu + n^\mu\right) + x^+\left(\bar{n}^\mu\right)\,, \tag{12}$$

where $\Omega_\mathrm{c}(x) = \Omega_\mathrm{c}(x^-)$ is the associated conformal factor and n_c and $\bar{n}_\mathrm{c}$ are mutually reciprocal $n_\mathrm{c}\cdot\bar{n}_\mathrm{c} = 1$ lightlike vectors. Elements of the lightsheet $\lim_{x^+\to 0}\mathrm{c}(x) = \Omega_\mathrm{c} n_\mathrm{c}$ may be coordinate transformed into standard spatio-temporal Minkowski space coordinates,

$$\Omega_\mathrm{c}(x^-)n_\mathrm{c}^\mu(\boldsymbol{x}_\perp) = \frac{1}{\lambda-x^-}\frac{1+\boldsymbol{x}_\perp^2}{2}\left[1e_0^\mu + \frac{2x^1}{1+\boldsymbol{x}_\perp^2}e_1^\mu + \frac{2x^2}{1+\boldsymbol{x}_\perp^2}e_2^\mu - \frac{1-\boldsymbol{x}_\perp^2}{1+\boldsymbol{x}_\perp^2}e_3^\mu\right]\,, \tag{13}$$

to reveal an extension to the stereographic projection presented in Eq. (8). $n_\mathrm{c}^0(\boldsymbol{x}_\perp)$ and $\Omega_\mathrm{c}(x^-)$ show parabolic and hyperbolic dependence on $\boldsymbol{x}_\perp$ and x^- respectively. Figure 5 showcases how the red/gray lightsheet is related to the green/light gray lightcone. Noting the signs of $\Omega_\mathrm{c}(x^-)$ — the past lightsheet $x^- < \lambda$ (Fig. 5 (b)) corresponds to the future lightcone and *vice versa* (Fig. 5 (c)). An x^--ordered trajectory on the whole lightsheet is unpreserved under the mapping onto the whole lightcone as showcased in Eq. (12).

A full correspondence of CGC and jet physics must therefore rely on a correspondence between half-infinite Wilson lines,

$$V_p \leftrightarrow U_{x;\lambda,-\infty} := P\exp\left[(-ig)\int_{-\infty}^{\lambda}\mathrm{d}x^- n_\mu b^{\mu a}(x)t^a_{(\mathrm{rep})}\right]\,. \tag{14}$$

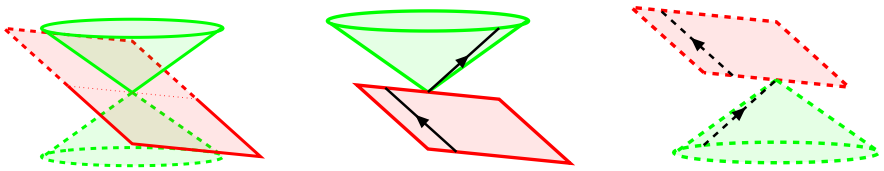

(a) Lightsheet geometry relates to lightcone geometry

(b) Past lightsheet and future lightcone. Trajectories relate causally

(c) Future lightsheet and past lightcone. Trajectories relate causally

Fig. 5. (Colour on-line) Graphical depiction of the relation between the (red/gray) lightsheet and (green/light gray) lightcone geometries established by HM map.

7. Conclusion

Equation (4b) indicates an equivalence of physical description of the evolution of the inclusive DIS cross section in the Regge–Gribov limit and the evolution of the semi-inclusive e^+e^- annihilation cross section within hard jets. The veto demonstrates proclivity for hard jets, such hard jets, however, do not demonstrate saturation-type behaviour. To encounter saturation-type physics in a jet measurement is fairly surprising — more so if the jets are created in empty space, for example in e^+e^- annihilation events [3].

The spatial correspondence of kernels and measures has been shown in Eq. (11). A spatio-temporal extension in Eq. (13) is used to characterize the geometric correspondence of the half-infinite Wilson lines in Eq. (14).

A full analysis shall appear in a Master's dissertation [12].

REFERENCES

[1] H. Weigert, *Nucl. Phys. A* **703**, 823 (2002).

[2] A. Banfi, G. Marchesini, G. Smye, *J. High Energy Phys.* **2002**, 006 (2002).

[3] H. Weigert, *Prog. Part. Nucl. Phys.* **55**, 461 (2005), arXiv:hep-ph/0501087.

[4] Y. Hatta, *J. High Energy Phys.* **2008**, 057 (2008).

[5] D.M. Hofman, J. Maldacena, *J. High Energy Phys.* **2008**, 012 (2008).

[6] F. Gelis, E. Iancu, J. Jalilian-Marian, R. Venugopalan, *Annu. Rev. Nucl. Part. Sci.* **60**, 463 (2010).

[7] R. Placakyte, arXiv:1111.5452 [hep-ph].

[8] E. Iancu, A. Leonidov, L.D. McLerran, *Nucl. Phys. A* **692**, 583 (2001).

[9] S.J. Brodsky, *AIP Conf. Proc.* **494**, 3 (1999).

[10] H. Weigert, *Nucl. Phys. B* **685**, 321 (2004).

[11] A. Vladimirov, *J. High Energy Phys.* **2018**, 045 (2018).

[12] J.A. Bohra, Master's Thesis, University of Cape Town, 2023.